chemosensors

Article

Evaluation Methods for Stability and Analysis of Underlying Causes of Instability in Form I Atorvastatin Calcium Drug Substance

Bo Chen [1], Zhilong Tang [1], Zhenxing Zhu [2], Yang Xiao [2], Guangyao Mei [2,*] and Xingchu Gong [1,3,4,*]

[1] College of Pharmaceutical Sciences, Zhejiang University, Hangzhou 310058, China; 22360539@zju.edu.cn (B.C.)
[2] Zhejiang Hongyuan Pharmaceutical Co., Ltd., Taizhou 317016, China
[3] Polytechnic Institute, Zhejiang University, Hangzhou 310015, China
[4] Jinhua Institute of Zhejiang University, Jinhua 321299, China
* Correspondence: mdmei@hongyuanpharm.com (G.M.); gongxingchu@zju.edu.cn (X.G.); Tel.: +86-13958539258 (G.M.); +86-571-88208427 (X.G.)

Abstract

Stability assessments of drug substances and the detection of crystalline forms are critical for ensuring drug quality and medication safety. Atorvastatin calcium drug substance samples were characterized using powder X-ray diffraction (PXRD) and differential scanning calorimetry (DSC). DSC results demonstrated a precise discrimination of the stability of samples. An analysis of PXRD characteristic peaks and DSC melting data suggested that instability likely stems from the presence of the amorphous phase. To validate this hypothesis, blended samples containing controlled ratios of amorphous phase and crystalline Form I were prepared. Quantitative models based on PXRD, DSC, and near-infrared spectroscopy (NIRS) data were developed to predict amorphous content, and classification accuracy was evaluated. Experimental results confirmed that all three models achieved classification accuracy values exceeding 70% in the stability prediction of the two groups of samples, which included "stable" and "unstable" samples, substantiating the hypothesis. Among them, the modeling method based on NIRS data was not only non-destructive and rapid but also demonstrates a superior discrimination accuracy value reaching 100% (n = 11), showing potential for promotion and application in industrial sample detection. The quantitative correlation between amorphous content and stability was successfully established in this study, offering a novel method for a quality stability assessment of atorvastatin calcium drug substances.

Keywords: atorvastatin calcium; amorphous; stability; near-infrared spectroscopy; partial least squares

check for updates

Received: 11 June 2025
Revised: 11 July 2025
Accepted: 14 July 2025
Published: 21 July 2025

Citation: Chen, B.; Tang, Z.; Zhu, Z.; Xiao, Y.; Mei, G.; Gong, X. Evaluation Methods for Stability and Analysis of Underlying Causes of Instability in Form I Atorvastatin Calcium Drug Substance. *Chemosensors* **2025**, *13*, 265. https://doi.org/10.3390/chemosensors13070265

Copyright: © 2025 by the authors. Licensee MDPI, Basel, Switzerland. This article is an open access article distributed under the terms and conditions of the Creative Commons Attribution (CC BY) license (https://creativecommons.org/licenses/by/4.0/).

1. Introduction

Atorvastatin calcium, whose systematic chemical name is R-(R*,R*)-2-(4-fluorophenyl)-β,δ-dihydroxy-5-(1-methylethyl)-3-phenyl-4-[(phenylamino)carbonyl]-1H-pyrrole-1-heptanoic acid hemi calcium salt, is a statin lipid-regulating drug. It was the first drug globally achieving annual sales of USD 10 billion [1]. Atorvastatin calcium can exist in different polymorphic forms [2], with Form I, Form II, and Form IV being the most common. Compared to other forms, Form I atorvastatin calcium exhibits superior stability and is essentially non-hygroscopic [3–5]. Consequently, Form I is the polymorph predominantly used commercially in the atorvastatin calcium drug substance.

Atorvastatin calcium can also exist in an amorphous form. Amorphous atorvastatin calcium is susceptible to heat, light, oxygen, and humidity, resulting in instability and a tendency to degrade, forming oxidation products [6,7]. These oxidation products act as impurities that can diminish the drug's efficacy. The amorphous form is also prone to transforming into other crystalline forms of atorvastatin calcium [8]. According to the provisions of the Pharmacopoeia of the People's Republic of China (2020 Edition), when a solid drug exhibits polymorphism and different crystalline forms may affect the effectiveness, safety, or quality of the drug, the qualitative or quantitative control of the crystalline form of the drug substance should be carried out [9]. Therefore, it is necessary to detect the crystalline form of the atorvastatin calcium drug substance.

An accurate evaluation of drug substance stability is crucial for ensuring the quality of the final dosage form and medication safety. Current stability evaluation methods primarily rely on accelerated and long-term testing [10]. However, these testing methods require at least six months to yield results, which is very time-consuming. Therefore, there is a need to develop a rapid method for identifying drug substance stability.

Traditional analytical techniques for polymorphic drugs include powder X-ray diffraction (PXRD), scanning electron microscopy (SEM), Fourier-transform infrared spectroscopy (FTIR), and thermal analysis techniques [11]. Shete et al. [12] utilized SEM, PXRD, and thermal analysis to characterize the crystalline and amorphous states of atorvastatin calcium and compared their differences. Salazar-Barrantes et al. [13] similarly employed PXRD, SEM, mid-infrared spectroscopy, and various thermal analysis techniques to study in detail the dehydration behavior and lattice changes in Form I atorvastatin calcium during heating. Some researchers have utilized Raman spectroscopy and near-infrared spectroscopy (NIRS) for the rapid detection of atorvastatin calcium, achieving quantitative content determination [14] and rapid measurement of physicochemical properties [15]. However, there is currently a lack of research on methods for detecting the proportion of the amorphous phase in the atorvastatin calcium drug substance.

Addressing the issue of stability identification in the atorvastatin calcium drug substance, samples with varying stability were first characterized by using PXRD and differential scanning calorimetry (DSC) in this study. Analysis of the PXRD characteristic peaks and thermodynamic data led to the preliminary hypothesis that the instability might originate from a heterogeneous system where the amorphous phase coexists with crystalline material. To verify this hypothesis, a detection method to determine the proportion of the amorphous phase in the sample was developed. Standard mixed samples of Form I atorvastatin calcium, containing different proportions of the amorphous phase, were prepared and analyzed using PXRD, DSC, and NIRS for method development, respectively. Therefore, this study aims to (1) establish mathematical models based on the acquired data to predict the proportion of the amorphous phase in the drug substance; (2) evaluate the classification accuracies of the models; and (3) verify the aforementioned hypothesis regarding the root cause of instability.

2. Materials and Methods

2.1. Material

The amorphous atorvastatin calcium and 11 batches of the Form I atorvastatin calcium drug substance were provided by Zhejiang Hongyuan Pharmaceutical Co., Ltd. (Taizhou, China). All samples were dried and hermetically stored in brown desiccators. Stability was defined by the company through a 6-month accelerated stability study conducted at 40 °C/75% relative humidity according to European Pharmacopoeia 10.7: batches with a content of oxidative impurity D $\leq$ 0.15% were classified as "stable" (S1–S4 in Table 1); conversely, batches with a content of oxidative impurity D $\geq$ 0.15% were classified as

"unstable" (US1–US7 in Table 1). Photos of the amorphous atorvastatin calcium and the Form I atorvastatin calcium drug substance are presented in Figure 1.

Table 1. The characteristics of Form I atorvastatin calcium drug substances.

Samples	Stability
S1	Stable
S2	Stable
S3	Stable
S4	Stable
US1	Unstable
US2	Unstable
US3	Unstable
US4	Unstable
US5	Unstable
US6	Unstable
US7	Unstable



(**a**) (**b**)

Figure 1. Atorvastatin calcium drug substance powder. (**a**) Amorphous atorvastatin calcium; (**b**) Form I atorvastatin calcium.

2.2. Sample Preparation

The amorphous sample and all of the Form I atorvastatin calcium samples from the 11 batches were appropriately ground and sieved to obtain particles within the size range of 0.100 mm–0.154 mm.

The stable sample (S2) and amorphous sample were weighed according to amorphous contents of 0%, 5%, 10%, 15%, 20%, and 30% then were placed into 5 mL polytetrafluoroethylene tubes. The tubes were mounted on a Rotating Mixer Shaker (model RMO-80, JOANLAB Equipment Co., Ltd., Huzhou, China). Every 30 min, the tubes were removed from the mixer shaker and shaken on a vortex mixer. Blending was performed for at least 3 h. The resulting mixed samples were designated as M0, M1, M2, M3, M4, and M5, respectively.

2.3. PXRD

PXRD testing was performed using a SmartLab X-ray powder diffractometer (SmartLab, Rigaku Corporation, Tokyo, Japan). Data were collected using Cu K_α radiation (λ = 1.54 Å). Samples ground uniformly to a fine powder using an agate mortar were prepared on glass sample holders. Measurements were conducted using a one-dimensional array detector with a tube voltage of 40 kV, tube current of 180 mA, and a 2θ scan range of 2° to 50° with a step size of 0.02°. The acquired data were processed using MDI Jade version 7.5.1 software.

2.4. DSC

Samples ground and sieved as described in Section 2.2 were analyzed using a differential scanning calorimeter (Mettler Toledo STARe System DSC3, Mettler-Toledo International Inc., Zurich, Switzerland). Approximately 2 mg of the sieved sample was placed in an unpierced aluminum crucible (unless otherwise specified). Analysis was performed under a heating rate of 10 K/min and a nitrogen atmosphere flow rate of 50 mL/min, covering a temperature range of 20–190 °C.

2.5. NIRS

Approximately 53 mg of the sieved sample from Section 2.2 was weighed and placed into a tablet die, where it was compressed into a round tablet (diameter 8 mm, Figure 2). Samples were measured using a near-infrared spectrometer equipped with a dual-polarization fiber optic reflection probe (ABB TALYS, ABB Ltd., Zurich, Switzerland). Detection conditions were as follows: number of scans, 32; resolution, 8 cm^{-1}; spectral range, 4000–12,000 cm^{-1}.



Figure 2. A round atorvastatin calcium tablet.

2.6. Data Processing

2.6.1. Data Preprocessing

Spectra often contain not only the chemical information of the sample itself but also extraneous information such as electrical noise, sample background, and stray light, which may interfere with result analysis. Therefore, appropriate preprocessing methods are required to reduce irrelevant information and noise in the spectral data [16,17]. Spectral preprocessing methods explored in this study include the standard normal variate (SNV), multiplicative scatter correction (MSC), first derivative (1stDer), and second derivative (2ndDer) [18].

2.6.2. Partial Least Squares (PLS)

Partial least squares (PLS) is a multivariate data analysis and predictive modeling method suitable for situations involving multicollinear independent and dependent variables. It constructs latent variables to explain the maximum covariance between the two sets of variables and is used to establish linear relationship models. The specific models are as follows:

$$X = TP^T + E_X \quad (1)$$

$$Y = UQ^T + E_Y \quad (2)$$

$$U = TB \quad (3)$$

where T and U are the score matrices of matrices X and Y, respectively; P and Q are the loading matrices of matrices X and Y, respectively; E_X and E_Y are the PLS residual matrices for X and Y, respectively; and B is the regression coefficient matrix for the linear regression of U on T. The matrix decomposition of X and Y is performed under the condition of maximizing the covariance between T and U [19].

PLS model indicators include R_X^2, R_Y^2, and Q^2. R_X^2 indicates the degree to which the PLS model explains the X variables and R_Y^2 indicates the degree to which the model explains the Y variables. Q^2 is the R^2 calculated based on the results of leave-one-out cross-validation. A higher Q^2 value indicates a better generalization performance of the model.

3. Results

3.1. PXRD Pattern Analysis

Figure 3 shows the PXRD patterns of the stable and unstable samples. Each batch of samples exhibits distinct characteristic diffraction peaks. The positions of these characteristic peaks are consistent with those reported in the 1999 US Patent 5969156 [4] and the literature [20]. Furthermore, no characteristic diffraction peaks of other polymorphic forms are present, indicating that both types of samples are Form I atorvastatin calcium and are not contaminated with other polymorphs. No significant differences are observed in the diffraction peak positions and relative intensities between the two types of samples.

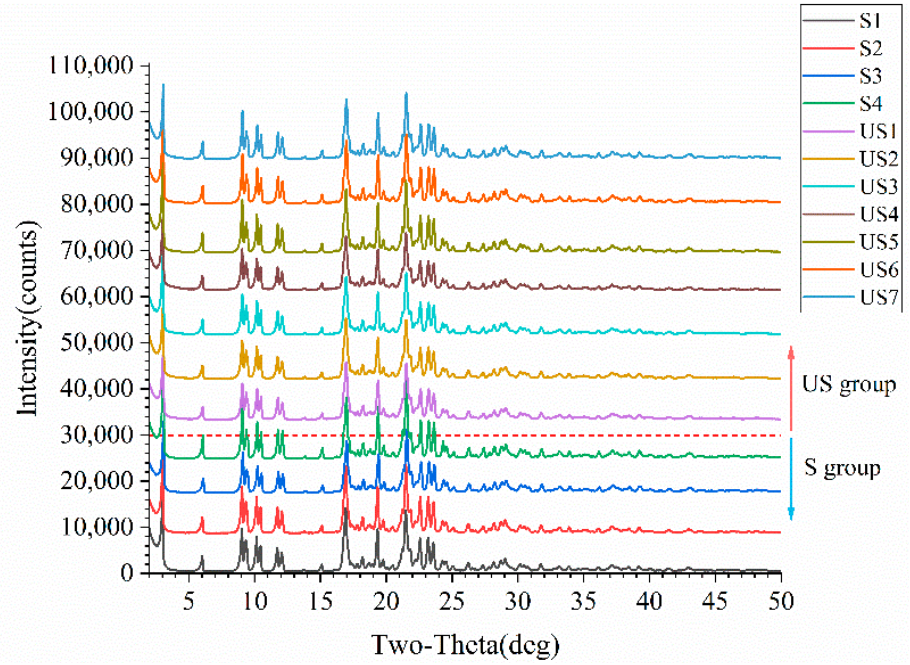

Figure 3. PXRD patterns of stable and unstable samples. The red dashed line divides the PXRD patterns of the two sample groups, with unstable (US) group samples above the line and stable (S) group samples below.

Figure 4 displays the PXRD patterns of amorphous and Form I atorvastatin calcium, revealing significant differences between them. The amorphous sample exhibits broad and diffuse diffraction peaks, indicating the absence of long-range order. In contrast, Form I displays a series of sharp Bragg diffraction peaks, confirming its highly ordered crystalline structure. Notably, the main diffraction peaks of Form I are concentrated within the 7.5°–25° (2θ) range. Within this angular range, the broadened diffraction peaks of the amorphous material partially overlap with the peaks of Form I. It is therefore hypothesized

that when Form I atorvastatin calcium contains a small amount of amorphous impurity, changes in the characteristic peaks of its PXRD pattern may be difficult to discern visually.

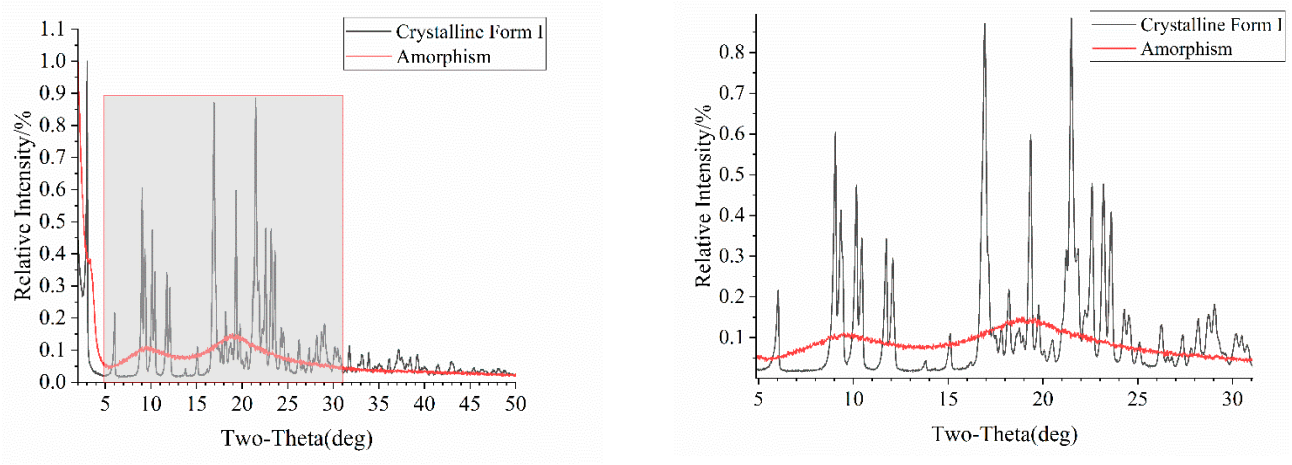

(**a**) (**b**)

Figure 4. PXRD patterns of Form I and amorphous atorvastatin calcium: (**a**) original figure with the gray area representing the enlarged portion; (**b**) enlarged figure.

The PXRD results of the mixed samples (Figure 5) confirm this hypothesis. The PXRD patterns indeed show no significant changes when Form I atorvastatin calcium is mixed with a small proportion of the amorphous phase.

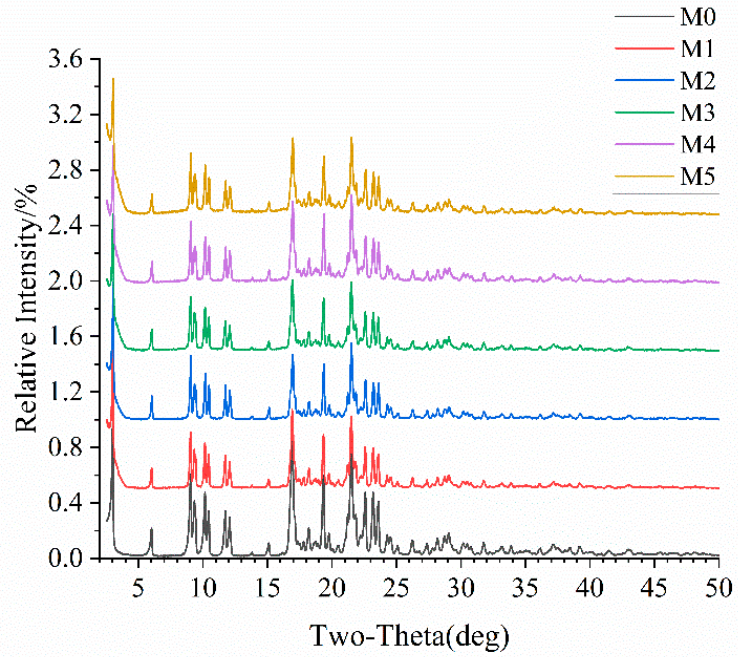

Figure 5. PXRD patterns of mixed samples. PXRD patterns from bottom to top correspond to samples with increasing amorphous content of 0%, 5%, 10%, 15%, 20%, and 30%, respectively.

3.2. Selection of DSC Measurement Method and Results

3.2.1. Selection of DSC Measurement Method

DSC provides thermodynamic information such as the melting point, glass transition temperature, and crystallinity of samples. DSC curves for Form I atorvastatin calcium have been reported in the literature [3,13]. However, different testing conditions can lead to

various DSC curves. Therefore, selecting appropriate testing conditions is necessary to obtain accurate and reliable experimental results.

The effect of using pierced versus unpierced crucibles on DSC measurements was investigated in this study. Figure 6 shows the DSC curves of Form I atorvastatin calcium under these two different testing conditions. The results indicate that when a pierced crucible was used (providing an open-system environment), two endothermic peaks appeared in the DSC curve: the first small endothermic peak corresponds to the heat absorption associated with the volatilization of the first bound water from Form I atorvastatin calcium trihydrate, while the second large endothermic peak corresponds to the heat absorption from the volatilization of the remaining two molecules of bound water and the melting endotherm of the anhydrous atorvastatin calcium (metastable phase). When an unpierced crucible (closed-system environment) was used, the DSC curve exhibited only one endothermic peak. This peak is attributed to the melting endotherm of Form I atorvastatin calcium trihydrate [21]. The DSC curve obtained under unpierced crucible conditions accurately reflects the melting point and enthalpy of fusion for Form I atorvastatin calcium. Consequently, subsequent DSC experiments were conducted using unpierced crucibles.

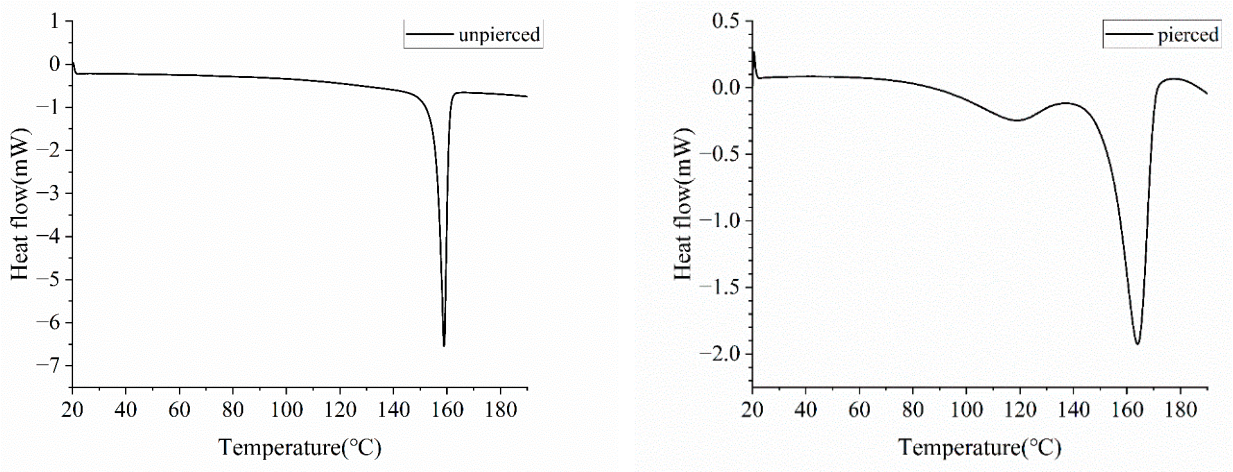

(**a**) (**b**)

Figure 6. DSC curves of Form I atorvastatin calcium. The crucible used for detection is (**a**) unpierced; (**b**) pierced.

3.2.2. Difference in Melting Point Between Stable and Unstable Samples

The DSC curves of stable and unstable samples are shown in Figure 7. The test data were integrated using STARe Default DB software (V16.00, Mettler Toledo, Zurich, Switzerland). The processing method was as follows: tangents were drawn from the two inflection points of the melting peak, intersecting the baselines before and after melting to determine the onset (start temperature of the melting peak) and endpoint. The temperature corresponding to the lowest point of the curve was automatically labeled as the peak temperature.

For pure, crystalline, low-molecular-weight substances, the onset temperature of the melting peak corresponds to the melting point [22,23]. The purity of the Form I atorvastatin calcium drug substance used in this study was above 99%. Therefore, the onset temperature of the melting peak was considered the melting point.

The melting points for samples in the S group and US group are summarized in Table 2. The relative absolute difference in measurements ranged between 0.0326–2.15% (see Appendix A Table A1), demonstrating good experimental repeatability. The box plots of these two datasets are presented in Figure 8. To test whether the melting points of the S group were significantly higher than those of the US group, significance testing was

performed using Minitab Statistical Software (Version 22, Minitab, LLC, State College, PA, USA). First, normality tests were conducted on both sample groups. The *p*-values for the statistical tests were 0.760 and 0.675, respectively. At a significance level of $\alpha = 0.05$, the melting point values of both groups were considered to follow a normal distribution. Subsequently, an F-test was used to determine the homogeneity of variances between the two populations. The result showed a *p*-value of 0.487, indicating equal population variances at $\alpha = 0.05$. Under the conditions of normal distribution and equal variance, a one-tailed *t*-test was performed to determine if the melting points of the S group were significantly higher than those of the UNS group. The statistical test yielded a *p*-value of 0.00007. At $\alpha = 0.05$, the null hypothesis was rejected, indicating that the melting points of the stable samples (S group) were significantly higher than those of the unstable samples (UNS group). Using a melting point threshold of 151 °C, the stability of atorvastatin calcium samples could be qualitatively distinguished.

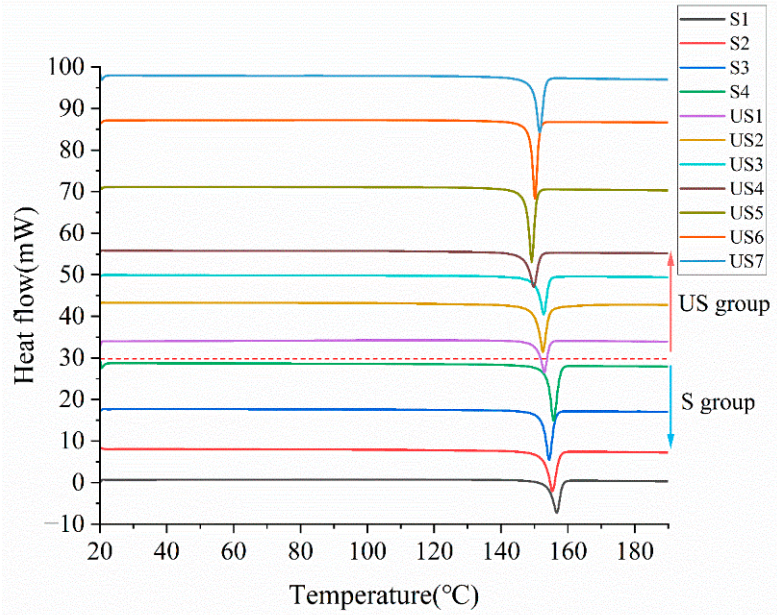

Figure 7. DSC curves of stable and unstable samples. The red dashed line separates the DSC curves of the two sample groups, with unstable (US) group samples above the line and stable (S) group samples below.

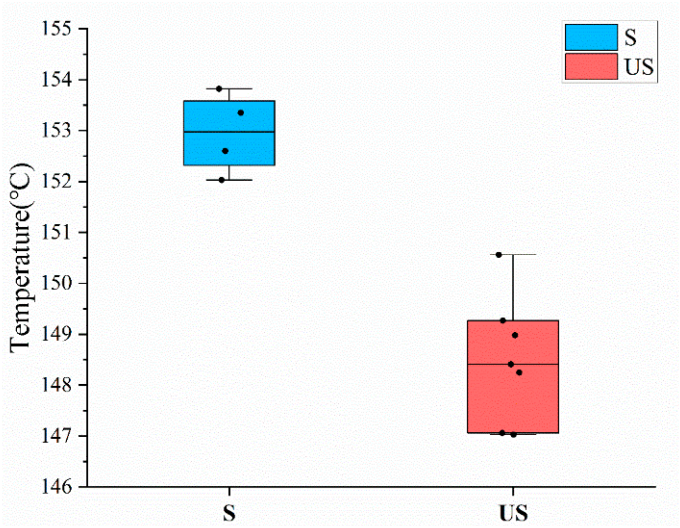

Figure 8. Box plot of samples in S group and US group. The bullets in the figure represent the melting point of each sample.

Table 2. Comparison of melting points of stable and unstable samples.

Samples	Melting Point/°C	Samples	Melting Point/°C
S1	153.82	US3	148.41
S2	152.60	US4	147.06
S3	152.03	US5	147.03
S4	153.35	US6	148.25
US1	150.56	US7	149.27
US2	148.98		

3.3. Analysis of Underlying Causes for Stability Differences in Drug Substance

The temperature of the phase transition (e.g., melting point, boiling point) should remain constant for a pure substance (chemical or polymorphic purity), which should exhibit a specific phase transition temperature [24]. Since the chemical purity of all 11 batches exceeded 99%, the significant difference in melting points indicates a difference in the polymorphic purity of the two types of samples. Specifically, the unstable samples have lower Form I polymorphic purity compared to the stable samples.

The chemical purity of all batches of samples was above 99%, so it was assumed that the content of other chemical impurities in the samples was extremely low, and their influence on the sample stability was ignored. Combined with the PXRD pattern analysis, it is hypothesized that the instability of the drug substance may originate from a heterogeneous system where the amorphous phase coexists with the crystalline phase. Due to the poor stability of amorphous material, a system containing both crystalline and amorphous phases is susceptible to oxidation reactions during storage or use. To verify this hypothesis, a detection method to determine the proportion of amorphous phase in a sample was developed. Standard mixed samples of Form I atorvastatin calcium, containing different proportions of the amorphous phase, were prepared (see Section 2.2) and analyzed using PXRD, DSC, and NIRS for method development, respectively. These mixed samples were analyzed by using PXRD, DSC, and NIR techniques. Mathematical models were established to predict the amorphous content in the 11 batch samples and to identify the optimal detection method.

3.4. Stability Identification of Atorvastatin Calcium Based on PXRD Data

To exclude the influence of factors such as instrument status, the relative intensity data of mixed samples' PXRD were preprocessed using SIMCA software (Version 14.1, Umetrics AB, Malmö, Sweden). A partial least squares (PLS) mathematical model was established, and the optimal model was determined using leave-one-out cross-validation. The relevant parameters of the PLS models are listed in Table 3.

Table 3. Parameters of PLS model based on PXRD data.

Model	Preprocessing Methods	Number of PLS Components	R_X^2	R_Y^2	Q^2
PXRD-M1	None	2	0.943	0.995	0.978
PXRD-M2	1stder	2	0.729	0.953	0.785
PXRD-M3	2ndDer	2	0.563	0.992	0.767
PXRD-M4	MSC	1	0.478	0.99	0.822
PXRD-M5	SNV	1	0.534	0.992	0.909
PXRD-M6	MSC-1stDer	2	0.609	0.999	0.845
PXRD-M7	SNV-1stDer	2	0.612	0.997	0.864

Q^2 is the coefficient of determination calculated from the leave-one-out cross-validation results. Since a higher Q^2 value indicates better model generalization per-

formance, PXRD-M1 was selected as the optimal model. The fitting effect of the model is shown in Figure 9. The prediction results for the amorphous content in the two types of samples are presented in Table 4.

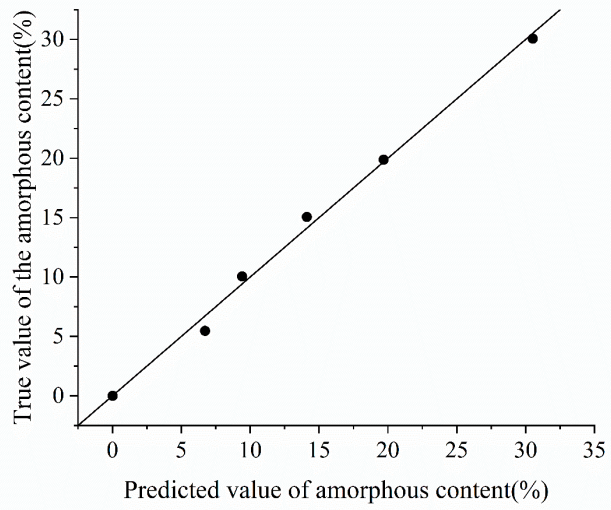

Figure 9. Fitting effect of PXRD-M1.

Table 4. The predicted value of the amorphous content for two types of samples based on PXRD-M1 model.

Samples	Predicted Value of the Amorphous Content/%	Samples	Predicted Value of the Amorphous Content/%
S1	0.623	US3	6.99
S2	0.0178	US4	16.9
S3	6.14	US5	3.19
S4	1.45	US6	3.44
US1	12.1	US7	9.21
US2	9.27		

To evaluate the classification performance of the model for the two types of samples, the following evaluation method was proposed: The classification threshold was defined as the average of the maximum predicted amorphous content value among stable samples and the minimum predicted amorphous content value among unstable samples. Samples with predicted amorphous content exceeding this threshold were classified as "unstable", while those below the threshold were classified as "stable". The model accuracy (A) was calculated using this method. The calculation formula is

$$A = \left(1 - \frac{a}{m}\right) \times 100\% \quad (4)$$

where m is the total number of samples and a is the number of misclassified samples. Based on the data in Table 4 and Formula (4), the classification accuracy of the PXRD-M1 model was calculated as 72.73%. The classification results were largely consistent with expectations.

3.5. Stability Identification of Atorvastatin Calcium Based on DSC Enthalpy of Fusion Data

The DSC curves of the mixed samples are shown in Figure 10. Table 5 presents the enthalpies of fusion calculated from the DSC curves for the stable samples, unstable samples, and mixed samples. Since the amorphous material does not exhibit a specific enthalpy of fusion (Figure 10), the enthalpies of fusion of the mixed samples should be linearly correlated with their amorphous content.

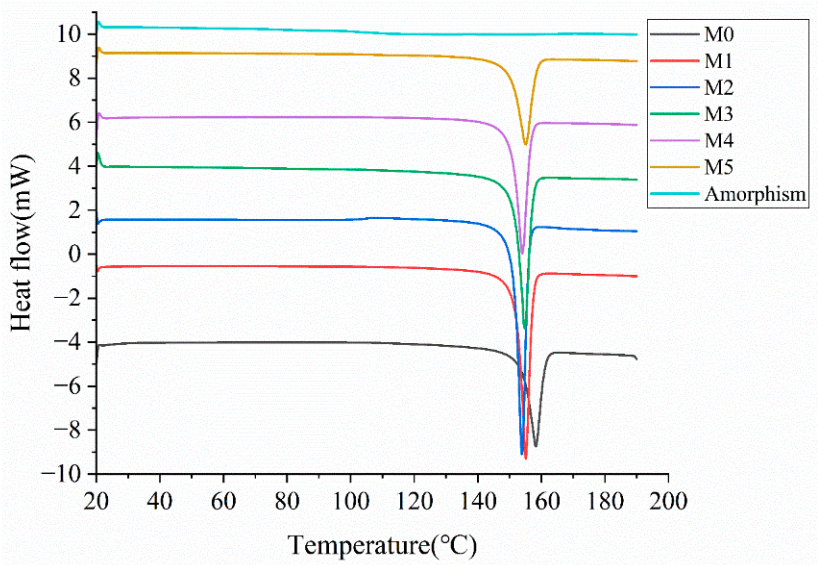

Figure 10. DSC curves of mixed samples. DSC curves from bottom to top correspond to mixed samples with amorphous content of 0%, 5%, 10%, 15%, 20%, 30%, and amorphous sample, respectively.

Table 5. Enthalpies of fusion of samples.

Samples	Enthalpy of Fusion/J/g	Samples	Enthalpy of Fusion/J/g	Samples	Enthalpy of Fusion/J/g
h0	−97.13	S1	−87.43	US3	−80.33
h1	−89.00	S2	−93.66	US4	−82.37
h2	−87.37	S3	−94.50	US5	−90.30
h3	−80.31	S4	−102.88	US6	−91.48
h4	−70.41	US1	−76.88	US7	−89.66
h5	−64.08	US2	−85.21	-	-

Therefore, linear Equation (5) was used to perform regression modeling between the enthalpy of fusion and the amorphous content in the mixtures:

$$y = b_0 + b_1 x \quad (5)$$

where y is the amorphous content of the sample, b_0 is the constant term, b_1 is the regression coefficient, and x is the enthalpy of fusion. The fitted values were b_0 = 83.05 ± 6.24 and b_1 = 0.8556 ± 0.0759. The model R^2 was 0.9695. The fitting effect is illustrated in Figure 11. The obtained model (designated DSC-M) was used to predict the amorphous content in the stable and unstable samples. The results are shown in Table 6. Using Formula (4), the model accuracy was calculated as 63.64%. While the classification results were largely consistent with expectations, the accuracy was not entirely satisfactory.

Table 6. Predicted value of the amorphous content based on enthalpies of fusion.

Samples	Predicted Value of the Amorphous Content/%	Samples	Predicted Value of the Amorphous Content/%	Samples	Predicted Value of the Amorphous Content/%
h0	−0.0544	S1	8.24	US3	14.3
h1	6.90	S2	2.91	US4	12.6
h2	8.30	S3	2.20	US5	5.79
h3	14.3	S4	−4.97	US6	4.78
h4	22.8	US1	17.3	US7	6.34
h5	28.2	US2	10.1		

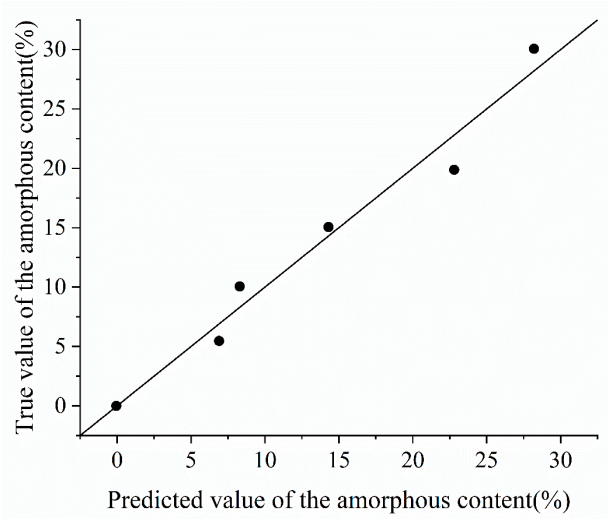

Figure 11. Fitting effect of DSC-M.

3.6. Stability Identification of Atorvastatin Calcium Based on NIRS Data

Figure 12 shows the NIRS spectra of the mixed samples. Similarly, the NIRS data of the mixed samples were preprocessed using SIMCA software. PLS mathematical models were established, and the optimal model was determined using leave-one-out cross-validation. The relevant parameters of the PLS models are listed in Table 7.

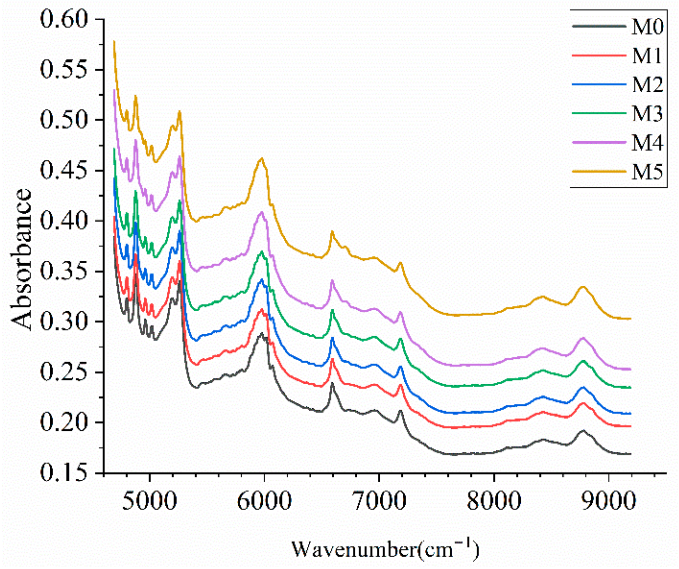

Figure 12. NIRS spectra of mixed samples. NIR spectra from bottom to top correspond to samples with increasing amorphous content of 0%, 5%, 10%, 15%, 20%, and 30%, respectively.

Table 7. Parameters of PLS model based on NIRS.

Model	Preprocessing Method	Number of PLS Components	R_X^2	R_Y^2	Q^2
NIRS-M1	1stDer	2	0.915	0.977	0.942
NIRS-M2	MSC	2	0.937	0.975	0.927
NIRS-M3	SNV	2	0.936	0.974	0.925
NIRS-M4	MSC-1stDer	2	0.892	0.982	0.941
NIRS-M5	SNV-1stDer	2	0.892	0.982	0.942
NIRS-M6	2ndDer	1	0.593	0.962	0.903

Based on the Q^2 values, NIRS-M1 and NIRS-M5 were selected as potential optimal models. The model fitting results are shown in Figure 13. Figure 14a,c display the NIRS spectra of the mixed samples after 1stDer and SNV-1stDer preprocessing, respectively. Figure 14b,d show enlarged views of the selected wavenumber range (5800–6850 cm^{-1}) in the spectra after the two preprocessing methods. The predicted results for the amorphous content in the two types of samples using both models are presented in Table 8.

Table 8. The predicted value of the amorphous content based on the NIRS-PLS model.

Samples	Predicted Value of the Amorphous Content/%	
	NIRS-M1	NIRS-M5
S1	0.734	2.70
S2	1.36	0.251
S3	4.54	6.31
S4	4.52	5.47
US1	6.47	5.24
US2	5.75	5.68
US3	6.16	6.04
US4	10.8	9.92
US5	7.92	7.30
US6	6.69	7.00
US7	10.2	9.01

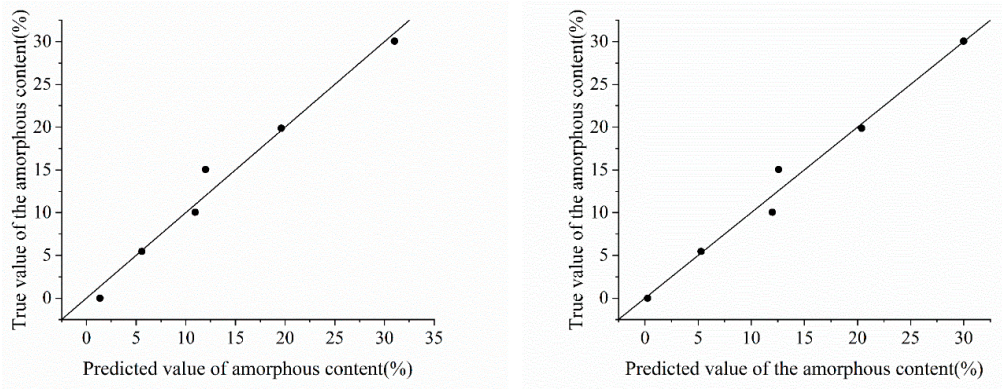

(**a**) (**b**)

Figure 13. Fitting effect of NIRS models. (**a**) NIRS-M1; (**b**) NIRS-M5.

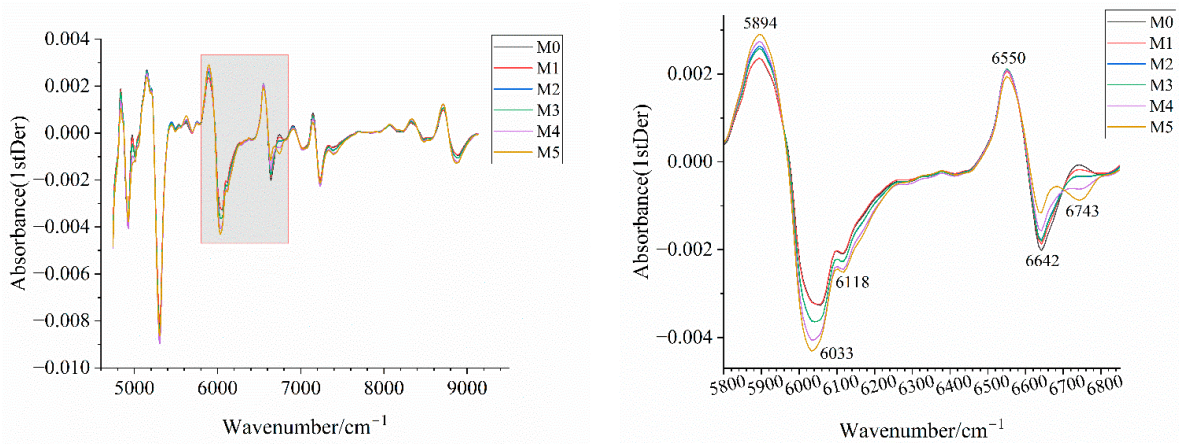

(**a**) (**b**)

Figure 14. *Cont.*

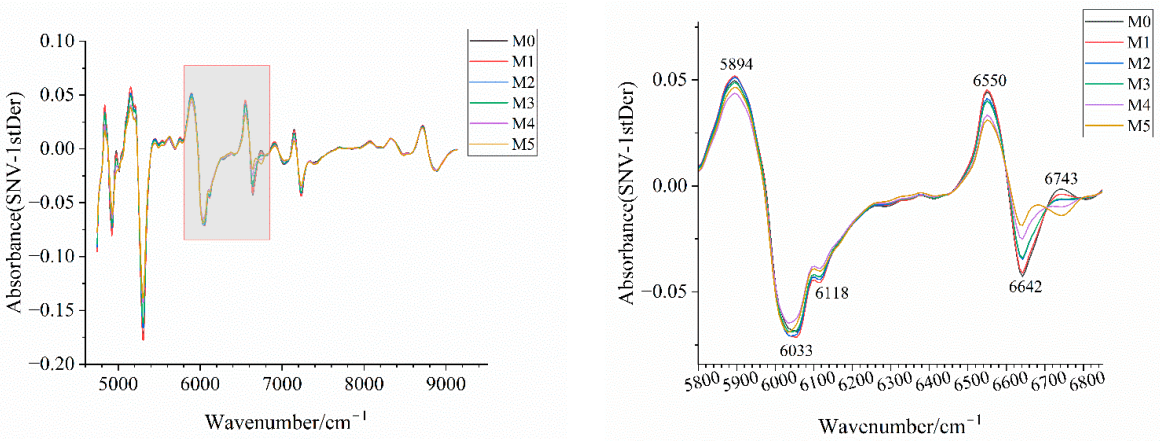

Figure 14. Near-infrared spectra of mixed samples after preprocessing. (**a**) Near-infrared spectrum after 1stDer preprocessing; (**b**) enlarged view of the wavenumber range 5800–6850 cm^{-1} in (**a**) with annotations highlighting the distinctive wavenumber regions among samples; (**c**) near-infrared spectra after SNV-1stDer preprocessing; (**d**) enlarged view of the wavenumber range 5800–6850 cm^{-1} in (**c**) with annotations highlighting the distinctive wavenumber regions among samples. M0–M5 correspond to mixed samples with an amorphous content of 0%, 5%, 10%, 15%, 20%, and 30%, respectively.

Based on the data in Table 8 and Formula (4), the classification accuracy for the NIRS-M1 and NIRS-M5 models were calculated as 100% and 72.73%, respectively. The results indicate that the NIRS-M1 model achieved perfect classification of the two sample types and was the optimal model obtained from the experiments.

4. Discussion

4.1. Prediction of Amorphous Content

Since the S2 sample was used as the Form I atorvastatin calcium component in all mixed samples, the predicted amorphous content values reported for the samples might be underestimated. This is because the Form I content in the S2 sample itself may not be 100% but potentially lower.

4.2. Discussion of Rationality of Hypothesis

The optimized models constructed based on PXRD, DSC, and NIRS techniques achieved classification accuracy exceeding 60% for both types of samples, as shown in Table 9. Notably, the NIRS-M1 model demonstrated 100% discrimination accuracy. This result indicates that the models built upon the hypothesis that "the instability of the drug substance may originate from a heterogeneous system where the amorphous phase coexists with the crystalline phase" can effectively distinguish samples with different stabilities. This provides evidence, to some extent, supporting the rationality of the hypothesis proposed in Section 3.3.

Table 9. Model accuracy for classifying between stable and unstable samples of the optimal model based on three detection techniques.

Model	Model Accuracy/%
PXRD-M1	72.73%
DSC-M	63.64%
NIRS-M1	100.0%
NIRS-M5	72.73%

4.3. Comparison of Three Detection Techniques

DSC enables precise sample classification based on melting point characteristics. However, its detection cycle is relatively long, and the high-temperature process can induce irreversible polymorphic transformations. PXRD allows for non-destructive testing and has a shorter detection time than DSC. Nevertheless, the classification model built using PXRD data exhibited relatively lower accuracy. NIRS technology, while achieving model classification accuracy comparable to DSC, offers the combined advantages of rapid detection and non-destructive analysis. Through a comprehensive evaluation of factors including detection efficiency, model performance, and sample integrity, this study concludes that NIRS technology demonstrates potential to become the superior analytical method among the three techniques for discriminating the polymorphic stability of the atorvastatin calcium drug substance.

4.4. Prediction of New Batches

Using the established NIRS-M1 model, we predicted the amorphous content of two newly produced batches, obtaining results of 1.44% and 4.70%, respectively. According to the classification threshold (5.145%) set by this model, both batches were classified as "stable". Similarly, manufacturers could utilize near-infrared spectroscopy (NIR) technology to rapidly assess the stability of each batch after the production of the atorvastatin calcium drug substance. If the model classifies a batch as "unstable", timely interventions could be implemented. This approach prevents stability issues from being detected only during long-term stability studies or even usage stages, thereby reducing quality control risks and testing costs, as well as shortening release cycles.

4.5. Selection of Classification Approach

This study adopts a method quantifying amorphous content to classify stable and unstable samples, as this approach provides direct physical interpretation. Another common strategy involves constructing classification models based on spectral data (e.g., using principal component analysis (PCA) or partial least squares discriminant analysis (PLS-DA)) to distinguish between stable and unstable batches. Although such models may achieve higher classification accuracy through a holistic consideration of all variables, they cannot clearly elucidate the intrinsic physical causes underlying the differences between the two sample types. Classification models often perform well when the sample size is sufficiently large and representative.

4.6. Limitations of Proposed Method

The method presented in this study still has some limitations. Firstly, the sample size used to establish the models (n = 11) is relatively small, and further validation with a larger sample size is required. Secondly, among the models established using three detection techniques based on the hypothesis, two failed to achieve 100% classification accuracy, which suggests that besides the heterogeneous system hypothesis proposed in this study, there may be other unidentified influencing factors. For example, these may include the impact of crystal morphology, distribution of the amorphous phase within the sample, and their microenvironment on sample stability. Subsequent research should employ multi-dimensional characterization techniques to systematically elucidate the underlying mechanisms of abnormal stability in the atorvastatin calcium drug substance.

5. Conclusions

An analysis of the PXRD patterns and information about the melting point from DSC for the amorphous and 11 batches of the Form I atorvastatin calcium drug substance

initially suggested that the instability of the drug substance might originate from a heterogeneous system where the amorphous phase coexists with the crystalline phase. The classification results obtained by predicting the proportion of the amorphous phase in the two types of samples using mathematical models established based on mixed samples further validated this conclusion. DSC analysis results can accurately distinguish between stable and unstable atorvastatin calcium drug substance samples. By comparing the three detection techniques—DSC, PXRD, and NIRS—it was determined that NIRS technology enables both rapid and non-destructive analysis while demonstrating superior performance in discriminating the stability of the atorvastatin calcium drug substance. This suggests its potential for further application in industrial product quality testing. In summary, the correlation between the proportion of the amorphous phase in the drug substance and its stability was established, providing a new perspective for research on the quality of the stability of the atorvastatin calcium drug substance. This approach holds significant practical value for ensuring drug efficacy and safety.

Author Contributions: Conceptualization, B.C., X.G., G.M., Z.Z. and Y.X.; methodology, X.G. and B.C.; validation, B.C.; formal analysis, B.C.; investigation, B.C. and Z.T.; resources, X.G. and G.M.; data curation, B.C., Z.Z. and Y.X.; writing—original draft preparation, B.C.; writing—review and editing, B.C., X.G. and Z.T.; visualization, B.C., Y.X. and Z.Z.; supervision, X.G. and G.M.; project administration, X.G. and G.M. All authors have read and agreed to the published version of the manuscript.

Funding: This research received no external funding.

Institutional Review Board Statement: Not applicable.

Informed Consent Statement: Not applicable.

Data Availability Statement: All data generated or analyzed during this study are included in the published article.

Acknowledgments: The authors are grateful to Haibin Qu for his suggestions.

Conflicts of Interest: Authors Zhenxing Zhu, Yang Xiao, and Guangyao Mei were employed by the company Zhejiang Hongyuan Pharmaceutical. The remaining authors declare that the research was conducted in the absence of any commercial or financial relationships that could be construed as potential conflicts of interest.

Appendix A

Table A1. The melting points of the samples in the two DSC measurements.

Number	Melting Point/°C		Relative Absolute Difference/%
	Measurement 1	Measurement 2	
S1	153.82	153.71	0.0715
S2	152.60	152.55	0.0328
S3	152.03	153.68	1.08
S4	153.35	153.40	0.0326
US1	150.56	150.68	0.0797
US2	148.98	150.25	0.849
US3	148.41	149.33	0.618
US4	147.06	147.56	0.339
US5	147.03	148.50	0.995
US6	148.25	151.47	2.15
US7	149.27	151.62	1.56

References

1. Skorda, D.; Kontoyannis, C.G. Identification and quantitative determination of atorvastatin calcium polymorph in tablets using FT-Raman spectroscopy. *Talanta* **2008**, *74*, 1066–1070. [CrossRef] [PubMed]
2. Jin, Y.S.; Ulrich, J. New Crystalline Solvates of Atorvastatin Calcium. *Chem. Eng. Technol.* **2010**, *33*, 839–844. [CrossRef]
3. Sonje, V.M.; Kumar, L.; Meena, C.L.; Kohli, G.; Puri, V.; Jain, R.; Bansal, A.K.; Brittain, H.G. Chapter 1—Atorvastatin Calcium//BRITTAIN H G. In *Profiles of Drug Substances, Excipients and Related Methodology*; Academic Press: San Diego, CA, USA, 2010; pp. 1–70.
4. Briggs, C.A.; Jennings, R.A.; Wade, R.W.; Harasawa, K.; Ichikawa, S.; Minohara, K.; Nakagawa, S. Crystalline [R-(R*, R*)]-2-(4-Dfluorophenyl)-β,δ-Dihydroxy-5-(1-Methylethyl)-3-Phenyl-4-[(Phenylamino)Carbonyl]-1H-Pyrrole-1-Heptanoic Acid Hemi Calcium Salt (Atorvastatin). U.S. Patent 5,969,156, 19 October 1999.
5. Gong, J.; Qin, C.; Hou, X.; Wu, S.; Hou, B. A Method for Crystallizing High-Purity Monodisperse Form I Atorvastatin Calcium in a Single Reactor. China CN201910862145.5, 19 April 2022.
6. El Kacemi, M.; El Orche, A.; El Bourakadi, K.; Benchekroun, Y.H.; Echerfaoui, F.; Karrouchi, K.; Bouatia, M.; El Karbane, M. Unveiling Impurities: A Comprehensive RP-HPLC Method for Accurate Atorvastatin Impurity Analysis in Pharmaceuticals Using an Accuracy Profile Approach. *J. AOAC Int.* **2024**, *107*, 735–748. [CrossRef] [PubMed]
7. Kračun, M.; Kocijan, A.; Bastarda, A.; Grahek, R.; Plavec, J.; Kocjan, D. Isolation and structure determination of oxidative degradation products of atorvastatin. *J. Pharm. Biomed. Anal.* **2009**, *50*, 729–736. [CrossRef] [PubMed]
8. Qin, C. Research on the Crystallization Process for Purification of Atorvastatin Calcium. Master's Thesis, Tianjin University, Tianjin, China, 2020.
9. Chinese Pharmacopoeia Commission. *Pharmacopoeia of the People's Republic of China: Volume IV: Guidelines for Polymorph Research and Quality Control of Crystalline Drugs: 9015*; China Medical Science and Technology Press: Beijing, China, 2020.
10. ICH. Stability Testing of New Drug Substances and Products: Q1A(R2). 2003. Available online: https://www.columbiapharma.com/reg_updates/international/ich/q1a.pdf (accessed on 10 July 2025).
11. Zhang, T. Research on Polymorphism and Spherical Crystallization of *Atorvastatin calcium*. Master's Thesis, Tianjin University, Tianjin, China, 2014.
12. Shete, G.; Puri, V.; Kumar, L.; Bansal, A.K. Solid State Characterization of Commercial Crystalline and Amorphous Atorvastatin Calcium Samples. *AAPS PharmSciTech* **2010**, *11*, 598–609. [CrossRef] [PubMed]
13. Salazar-Barrantes, K.A.; Vega-Baudrit, J.R.; Navarro-Hoyos, M.; Araya-Sibaja, A.M. Thermoanalytical techniques applied to the solid-state characterization of atorvastatin calcium trihydrate form I. *Chem. Thermodyn. Therm. Anal.* **2024**, *14*, 100130. [CrossRef]
14. Lim, Y.-I.; Han, J.; Woo, Y.-A.; Kim, J.; Kang, M.J. Rapid quantitation of atorvastatin in process pharmaceutical powder sample using Raman spectroscopy and evaluation of parameters related to accuracy of analysis. *Spectrochim. Acta A Mol. Biomol. Spectrosc.* **2018**, *200*, 26–32. [CrossRef] [PubMed]
15. Kobayashi, M.; Hattori, Y.; Sasaki, T.; Otsuka, M. Near-Infrared Spectroscopy-Based Nondestructive At-Line Analysis of Physico-Chemical Properties of Atorvastatin Calcium Hydrate after Grinding. *J. Drug Deliv. Sci. Technol.* **2022**, *71*, 103266. [CrossRef]
16. Rinnan, A. Pre-processing in Vibrational Spectroscopy—When, Why and How. *Anal. Methods* **2014**, *6*, 7124–7129. [CrossRef]
17. Engel, J.; Gerretzen, J.; Szymańska, E.; Jansen, J.J.; Downey, G.; Blanchet, L.; Buydens, L.M. Breaking with trends in pre-processing? *TrAC Trends Anal. Chem.* **2013**, *50*, 96–106. [CrossRef]
18. Rinnan, Å.; van den Berg, F.W.J.; Engelsen, S.B. Review of the Most Common Pre-Processing Techniques for Near-Infrared Spectra. *TrAC Trends Anal. Chem.* **2009**, *28*, 1201–1222. [CrossRef]
19. Chu, X. *Chemometric Methods in Modern Spectral Analysis*; Chemical Industry Press: Beijing, China, 2022.
20. Hodge, R.L.; Kaduk, J.A.; Gindhart, A.M.; Cheung, W.; Yu, S.; Kurtz, C.; Jasinski, J.B. Crystal structure of atorvastatin calcium trihydrate Form I (Lipitor®), $(C_{33}H_{34}FN_2O_5)_2Ca(H_2O)_3$. *Powder Diffr.* **2020**, *35*, 136–143. [CrossRef]
21. Tizaoui, C.; Galai, H.; Barrio, M.; Clevers, S.; Couvrat, N.; Dupray, V.; Coquerel, G.; Tamarit, J.-L.; Rietveld, I.B. Does the trihydrate of atorvastatin calcium possess a melting point? *Eur. J. Pharm. Sci.* **2020**, *148*, 105334. [CrossRef] [PubMed]
22. *E793-24*; Standard Test Method for Enthalpies of Fusion and Crystallization by Differential Scanning Calorimetry. ASTM International: West Conshohocken, PA, USA, 2024.
23. *E794-24*; Standard Test Method for Melting And Crystallization Temperatures By Thermal Analysis. ASTM International: West Conshohocken, PA, USA, 2024.
24. Chinese Pharmacopoeia Commission. *Pharmacopoeia of the People's Republic of China: Volume IV: Thermal Analysis: 0661*; China Medical Science and Technology Press: Beijing, China, 2020.

Disclaimer/Publisher's Note: The statements, opinions and data contained in all publications are solely those of the individual author(s) and contributor(s) and not of MDPI and/or the editor(s). MDPI and/or the editor(s) disclaim responsibility for any injury to people or property resulting from any ideas, methods, instructions or products referred to in the content.